https://doi.org/10.5194/cp-2022-76
Preprint. Discussion started: 18 November 2022

Climate of the Past
Discussions
Open Access

South Asian summer monsoon enhanced by the uplift of Iranian Plateau in Middle Miocene

Meng Zuo[1], Yong Sun[2], Yan Zhao[2*], Gilles Ramstein[3], Lin Ding[2], Tianjun Zhou[1]

1 State Key Laboratory of Numerical Modeling for Atmospheric Sciences and Geophysical Fluid Dynamics, Institute of Atmospheric Physics, Chinese Academy of Sciences, Beijing 100029, China

2 Key Laboratory of Continental Collision and Plateau Uplift, Institute of Tibetan Plateau Research, and Center for Excellence in Tibetan Plateau Earth Sciences, Chinese Academy of Sciences, Beijing 100101, China

3 Laboratoire des Sciences du Climat et de l'environnement, CNRS-CEA-UVSQ, 91191 Gif-sur-Yvette, France

Correspondence to: Yan Zhao (yan.zhao@itpcas.cn)

https://doi.org/10.5194/cp-2022-76
Preprint. Discussion started: 18 November 2022

Abstract. The South Asian summer monsoon (SASM) remarkably strengthened during the Middle Miocene (16-11 Ma), coincident with the rapid uplifts of the Iranian Plateau (IP) and the Himalaya (HM). Although the development of the SASM has long been linked to the topographic changes in the Tibetan Plateau (TP) region, the effects of the HM and IP uplift are still vigorously debated, and the underlying mechanisms remain unclear. Based on Middle Miocene paleogeography, we employ the fully coupled earth system model CESM to perform a set of topographic sensitivity experiments with altered altitudes of the IP and the HM. Our simulations reproduce the strengthening of the SASM in northwestern India and over the Arabian Sea, largely attributing to the thermal effect of the IP uplift. The elevated IP insulates the warm and moist airs from the westerlies in the south of the IP and produces a low-level cyclonic circulation around the IP, which leads to the convergence of the warm and moist air in the northwestern India and triggers positive feedback between the moist convection and the large-scale monsoon circulation, further enhancing the monsoonal precipitation. Whereas the HM uplift produces orographic precipitation without favorable circulation adjustment for the SASM. We thus interpret the intensification of the Middle Miocene SASM in the western part of the South Asia as a response to the IP uplift while the subtle SASM change in eastern India reflects the effects of the HM uplift.

Key words: South Asian summer monsoon, Middle Miocene, topographic change, thermal heating effect

https://doi.org/10.5194/cp-2022-76
Preprint. Discussion started: 18 November 2022

1. Introduction

There is increasing evidence of the inception/intensification of the South Asian Summer monsoon (SASM) during the middle Miocene (Clift et al., 2008; Gupta et al., 2015; Zhuang et al., 2017). The growth of the Tibetan Plateau (TP) and the surrounding orography has long been called for the SASM development (Manabe and Terpstra, 1974; Kutzbach et al., 1989; Prell and Kutzbach, 1992; Ramstein et al., 1997; An et al., 2001; Kitoh, 2002; Chakraborty et al., 2006; Wu et al., 2012; Tarif et al., 2020) although other factors such as geography and CO_2 concentration may also play important roles (Ramstein et al., 1997). Coincident with the rapid uplift during the Miocene, the Himalayas (HM) and the Iranian Plateau (IP) draw particular attention (Boos and Kuang, 2010; Zhang et al., 2012; Tang et al., 2013; Zhang et al., 2015; Acosta and Huber, 2020), but their effects on SASM and the underlying mechanisms are vigorously debated. In particular, the HM that has long been regarded as the "southern TP" (Spicer, 2017) receives more attention than the IP. Some studies showed that the narrow orography of the HM and the western mountain ranges were sufficient to reproduce the large-scale SASM circulation (Boos and Kuang, 2010; Zhang et al., 2012; Ma et al., 2014). Others (Zhang et al., 2015; Farnsworth et al., 2019; Acosta and Huber, 2020) argued that the uplift of the HM had little impacts on the monsoonal precipitation (Zhang et al., 2015; Acosta and Huber, 2020) while the IP played a more important role.

Concerning the influence of the IP and/or the HM uplift on the SASM, different mechanisms were proposed. Some researchers emphasized the insulation effect (Boos and Kuang, 2010; Ma et al., 2014) in that the elevated HM and IP prevent the high-enthalpy air in northern India from the cold and dry extratropics. Others highlighted the effect of sensible heating (Wu et al., 2012, henceforth Wu12) because strong monsoonal precipitation cannot occur without sensible heating even if the pool of high-enthalpy air is blocked in northern India. Tang et al. (2013, henceforth Tang13) demonstrated that the mechanical blocking effect contributed more to monsoonal precipitation than the sensible heating effect did. The divergent effects among these studies partially resulted from the experimental design which reflected different geological evolution of the TP region. It is thus important to estimate the SASM response to orographic change in the context of "realistic" geological history.

The topography evolution in the TP region is complex, spatially heterogenous and controversial (Wang et al., 2014; Botsyun et al., 2019; Ding et al., 2022). But most of the recent studies agreed that the elevated TP except its north well existed before the Miocene (Wang et

https://doi.org/10.5194/cp-2022-76
Preprint. Discussion started: 18 November 2022

al., 2014). The geologic evidence also suggests that the uplift of the IP (McQuarrie et al., 2003; Mouthereau, 2011; Ballato et al., 2017; Bialik et al., 2019) and the HM (Ding et al., 2015) occurred approximately at the same period as the Miocene SASM enhancement around 15-12 Ma (Clift et al., 2008; Gupta et al., 2015; Zhuang et al., 2017). These advances in geology not only provide improved topography constrain for the middle Miocene climate modeling, but also motivate us to revisit the impacts of the IP and HM uplift on the SASM as well as the underlying mechanism.

So far, a vast majority of modeling studies have focused on sensitivity experiments associated with modern geographies and neglected the geological history in the TP region, which may lead to a misleading interpretation for past changes because the geography has significant impacts on Asian climate (Ramstein et al., 1997; Fluteau et al., 1999; Farnsworth et al., 2019; Tarif et al., 2020). Meanwhile, only if the model simulation corresponds to special geology epoch, the results can be compared with the reconstruction proxies straightforwardly. Most of the topographic sensitivity experiments were conducted with Atmospheric general circulation model (AGCM) only, but the process of air–sea interaction should not be ignored since the large-scale mountains such as the TP significantly influences the oceanic circulations and the associated changes in the Asian climate (Kitoh, 2002; Su et al., 2018). Therefore, it is worthy to revisit the SASM response to the IP and HM uplift under Miocene boundary conditions as well as the underlying mechanism with fully couple climate model.

In this study, a fully coupled earth system model is employed to explore the impact of the IP and HM uplift on the SASM. The topographic sensitivity experiments are placed into the context of the current understanding of the regional tectonic and geographic settings. The model configuration, middle Miocene boundary condition and experimental design are described in Section 2. In Section 3, we show the SASM response to the IP and HM uplift. The mechanisms responsible for the monsoonal precipitation change are examined in Section 4. The implication of our results to the evolution of the SASM in the middle Miocene is discussed in Section 5 before giving conclusions in Section 6.

2. Data and Methods

2.1. Climate model

The model used in this study is the Community Earth System Model (CESM), Version 1.2.1 of the National Center for Atmospheric Research. It includes the Community Atmosphere

https://doi.org/10.5194/cp-2022-76
Preprint. Discussion started: 18 November 2022

Model (CAM4) (Neale et al., 2013), the Community Land Model (CLM4; Hunke and Lipscomb, 2010) the Parallel Ocean Program (POP2; Smith et al., 2010), the Community Ice Sheet Model and the Community Ice code (Glimmer-CICE4). The horizontal resolution used is 1.9°(latitude) × 2.5° (longitude) for CAM4 with 26 vertical levels and CLM4 has identical horizontal resolution. CESM has been extensively used for modern and the tectonic climate studies (Chen et al., 2014; Goldner et al., 2014; Frigola et al., 2018). In general, this model simulates modern surface temperature distributions and equator-to-pole temperature gradients well (Gent et al., 2011), although biases exist (Neale et al., 2013). However, it strongly overestimates the Miocene meridional temperature gradient compared to reconstructions, a thorny problem for Miocene modeling practice (Burls et al., 2021; Steinthorsdottir et al., 2021) mainly caused by the inability of reproducing polar amplified warmth (Krapp and Jungclaus, 2011; Herold et al., 2011; Goldner et al., 2014; Burls et al., 2021). Nevertheless, the temperature biases in low latitudes are small, generally within 1°C (Burls et al., 2021).

2.2. Boundary conditions

The core boundary conditions for running global general circulation models include topography, bathymetry and vegetation. Our experiments are configured with topography and bathymetry from Frigola et al. (2018, henceforth F18) which intend to provide boundary conditions for modeling studies with a focus on the Middle Miocene. According to F18, the most prominent geographic differences between Middle Miocene and present day are the opening of the Tethys, Indonesian and Panama seaways, the closure of the Bering Strait and lower elevations of most of the highest regions of the globe.

Concerning topography in the Tibetan Plateau, F18 is set with estimated Early to Middle Miocene elevation. The southern and central plateau reached a near modern elevation, the northern plateau is set to 3-4 km but its northward extend is reduced to reflect the rapid uplift occurring in Pliocene (Harris, 2006, and the references therein). To its west, the northern part of the IP reached a near modern elevation as 1000-2000 m. The HM reached to 60-80% of its present height. In general, the topography in F18 reasonably represents the uplifting features of the Tibetan Plateau at middle Miocene.

2.3. Experimental design

We first use CESM to perform two simulations: the pre-industrial (piControl) and the Middle Miocene (MMIO) simulation, which differ in their applied geography (Figs. 1a and b)

https://doi.org/10.5194/cp-2022-76
Preprint. Discussion started: 18 November 2022

and the CO_2 concentrations. The piControl use modern geography and the CO_2 concentration is set to 280 ppmv (Eyring et al., 2016) while the MMIO use the F18 boundary condition and CO_2 concentration is set to 400 ppmv. Both simulations are integrated to reach quasi-equilibrium, particularly the MMIO experiment is integrated over 3000 years. The difference between the two experiments provides the background information on the simulated total changes in the SASM between the two periods.

Based on MMIO simulation, we run a set of experiments with altered orography in the HM and the IP. Here we lumped together all the mountain ranges west of the Himalayan front, which include the Hindu Kush region and Pamir as the IP. We examine the joint effects of the HM and the IP on the SASM assuming the HM and the IP rise simultaneously from flat (0%) to 100% of their reference height (Figs. 1c and d). The reference height is the modern altitude for the HM and the reconstructed Miocene altitude for the IP. The experiments are referred as IP0HM0 and IP100HM100, respectively. We note that the IP and HM in the MMIO simulation reach 100% and 80% of their reference height, respectively, thus the MMIO experiment is equivalently referred as IP100HM80. The difference between IP100HM100 and MMIO reflects the climatic effect of the HM projecting above the TP.

To further separate the climatic effect of the IP and HM uplift, we conduct another two experiments: IP0HM100 and IP100HM0. In the former (latter) experiment, the IP (HM) is absent while the HM (IP) reaches its reference height (Figs.1e and f). The climate response to IP uplift is thus estimated as ((IP100HM0 – IP0HM0) + (IP100HM100 – IP0HM100))/2. Similarly, the effect of HM uplift is estimated as ((IP0HM100 – IP0HM0) + (IP100HM100 – IP100HM0))/2. The above sensitivity experiments are integrated over 200 years with CESM reaching quasi-equilibrium. The last 50 years are used for analysis.

2.4 Moisture budget analysis

Moisture budget analysis can decompose the precipitation into changes in evaporation and moisture advection. We apply the moisture budget analysis to reveal the physical processes related to SASM precipitation responses to the uplift of IP-HM (Chou et al. 2009). The moisture budget is written as:

$$P' = -<\omega\partial_p q>' - <\mathrm{V}\cdot\nabla \mathrm{q}>' + E' + residual \qquad (1)$$

Where the angle bracket < > means a mass integration through the troposphere, the primes $'$ represent the difference between experiments with and without the uplift of IP and HM. P and

https://doi.org/10.5194/cp-2022-76
Preprint. Discussion started: 18 November 2022

Climate of the Past
Discussions

E denote precipitation and evaporation, respectively. V and ω represent horizontal wind and vertical pressure velocity, respectively. And q is specific humidity. $<\omega\partial_p q>'$ and $<V\cdot\nabla q>'$ represent vertical moisture advection and horizontal moisture advection, respectively, and can be further divided into the thermodynamic and dynamic terms:

$$-<\omega\partial_p q>' = -<\overline{\omega}\partial_p q'> - <\omega'\partial_p\overline{q}> - <\omega'\partial_p q'> \qquad (2)$$

$$-<V_h\cdot\nabla q>' = -<\overline{V_h}\cdot\nabla q'> - <V_h'\cdot\nabla\overline{q}> - <V_h{}'\cdot\nabla q'> \qquad (3)$$

$-<\omega'\partial_p\overline{q}>$ and $-<V_h'\cdot\nabla\overline{q}>$ are dynamic terms related to changes in circulation, while $-<\overline{\omega}\partial_p q'>$ and $-<\overline{V_h}\cdot\nabla q'>$ are thermodynamic terms related to changes in specific humidity.

3. Results

3.1. Model performance

The CESM was estimated as one of the best performing models in terms of SASM simulations for present-day (Anand et al., 2018; Jin et al., 2020). Compared to the observation-based data GPCP (precipitation)/ERA5 (circulation) (Huffman et al., 2009; Hersbach et al. 2020), the CESM successfully simulated the broad features of the SASM system including the onshore flows and strong monsoonal precipitation. The maximum centers of precipitation are reasonably captured over the southern slope of the HM, the East Arabian Sea and Bay of Bengal despite biases in intensity and extensions. The All Indian rainfall (AIR), regional mean precipitation over the land points within the domain (7-30°N, 65-95°E), is 7.7 mm day^{-1} in GPCP and 8.7 mm day^{-1} in piControl experiment.

Compared with the piControl experiment, the MMIO simulation displays apparent adjustment of the JJA mean low-level circulation. The westerlies pass Africa and move into the Indian region and a cyclonic circulation develops over the Arabian Sea, the meridional cross-equatorial flow weakens and displaces southward (Fig. 2c). There is considerable enhancement of monsoonal precipitation in South Asia but not limited there (Fig. 2c). The regional mean precipitation AIR is 10.4 mm day^{-1}, ~20% higher than piControl experiment. The wetter Miocene climate is also reflected by the widespread Africa-Asian monsoon. Here a monsoon-like climate is defined as local summer-minus-winter precipitation exceeding 2 mm day^{-1} and the local summer precipitation exceeding 55% of the annual total (Wang and Ding, 2008). This monsoon index is determined by the intensity of summer monsoonal precipitation in the region of the South Asian Monsoon (SAM). Compared with present day, the domain of the SAM

https://doi.org/10.5194/cp-2022-76
Preprint. Discussion started: 18 November 2022

Climate of the Past Discussions

extends westward both in land and over the Arabian Sea where it nearly connects the African monsoon (Fig. 3c), a feature also presented in the study of Fluteau et al. (1999). The distribution of the simulated SAM is generally consistent with the proxies (Table 1). We note that the sites ODP 359 and 758 are located at low latitude (ca 5° N) where monsoon-like precipitation seasonality is absent, but they reflect the seasonal reverse of SAM wind regime (Betzler et al., 2016) and variability of precipitation in the Bay of the Bengal (Ali et al., 2017), respectively. The westward expansion of the SAM in the northwestern India is supported by the humid middle Miocene climate where the environment was dominated by C3 woodlands instead of today's C4 grasslands (Quade et al., 1989). In brief, the reasonable agreements between the piControl experiment and the observations as well as between the MMIO experiment with the paleo-reconstructions give us confidence on the use of CESM as a valid tool to study the impact of topography on the SASM.

3.2. The effect of the HM and IP uplift

We first examine the effect of the joint uplift of the HM and IP (hereafter referred to as IP-HM). With the uplift of the IP-HM (Fig. 4a), a prominent cyclonic anomaly is built to the west of the IP with the intensified southwesterlies from Africa via the Arabian Sea into the northwestern India. Increased precipitation is found along the eastern flank of the cyclonic anomaly. In the eastern part of the monsoon region, the enhancement of precipitation occurs mainly along the southern edge of the HM while the leeward side features a remarkably decreased precipitation, indicating the rain shadow effect. Corresponding to the summer precipitation change in response to the uplift of the IP-HM, the domain of the SASM expands westward over the Arabian Sea and the Indian subcontinent (Figs. 3d-e). The western extension over land is about 65 °E in the IP0HM0 experiment and reaches 60°E in the IP100HM100 experiment, indicating that the change of the SASM is significant in the region to the west of the HM.

We further separate the effect of the IP and HM uplift. With the uplift of the IP (Fig. 4b), the precipitation significantly increases in the region to the west of the HM but little change in the eastern part. The changes in precipitation and low-level circulation much resemble that attributing to the uplift of IP-HM (Fig. 4a), indicating that by itself, the IP can sustain major parts of the precipitation changes except over the central-eastern HM. The easterly anomaly across the Indian subcontinent indicates the westerly is blocked by elevated IP from northern India, facilitating moisture convergence and rainfall over the northern Indian continent. In

https://doi.org/10.5194/cp-2022-76
Preprint. Discussion started: 18 November 2022

contrast to the widespread effect of the IP on the SASM, the HM uplift only has a local effect (Fig. 4c), which is mostly confined to the HM and its close vicinity, and the change in low level circulation is noisy and weak. The precipitation strongly increases along the southern slope of the HM and dramatically decreases on its leeward side, resembling the changes in precipitation in the eastern region caused by the IP-HM uplift. In brief, the joint influences of the IP-HM uplift on the SASM are the superimposed effect of the IP and HM. In the western region, i.e., from the Arabian Sea to the northwestern India and Pakistan, the IP plays a dominant role while in the eastern region, i.e., the east part of South Asia, the changes in the SASM mainly attribute to the HM uplift.

4. Mechanisms

4.1. Moisture budget analysis

We interpret the regional precipitation changes attributing to the uplift of the IP and HM with the moisture budget decomposition, which relates the net precipitation (precipitation minus evaporation; P - E) to the vertically integrated moisture flux convergence (Chou et al., 2009). Figure 5a shows the moisture budget for precipitation changes caused by the IP uplift. The increased precipitation (2.0 mm day^{-1}) largely attributes to the horizonal moisture advection (2.1 mm day^{-1}) while the vertical advection plays a secondary role (1.1 mm day^{-1}). Further decomposition reveals that the moisture advection by anomalous meridional winds $-< \mathrm{v}' \cdot \partial_y \overline{q} >$ (Fig. 5f) significantly contributes to enhanced precipitation in the wide domain around the Arabian Sea and the IP region. However, its spatial pattern is some different from that of precipitation anomaly (Fig. 5b), indicating the contributions from other thermodynamic and dynamic terms cannot be neglected (Fig. 5a). For instance, the thermodynamic term related to specific humidity change $-< \overline{\omega} \partial_p \mathrm{q}' >$ significantly contributes to the precipitation anomaly in the western edge of the HM (Fig. 5c). The eastward advection of anomalous moisture from Arabian Sea $-< \overline{u} \partial_x \mathrm{q}' >$ (Fig. 5e) and the dynamic term related to vertical motion anomalies $-< \omega' \partial_p \overline{q} >$ (Fig. 5d) contribute to the enhanced precipitation over the western coast of India. We speculate that the enhanced precipitation in the western region results from the large-scale anomalous meridional moisture advection interaction with regional orography.

In contrast to the effect of the IP uplift, precipitation change caused by the HM uplift is relatively small (1.2 mm day^{-1}, accounting for 15% of precipitation in HM0 experiment). It is mainly caused by the vertical moisture advection and is offset by the horizontal moisture

https://doi.org/10.5194/cp-2022-76
Preprint. Discussion started: 18 November 2022

Climate of the Past
Discussions

advection. The spatial distribution of the dynamic term $-<\omega'\partial_p\overline{q}>$ (Fig. 6c) closely resemble that of precipitation change but its contribution is little, indicating that the uplift of the HM shifts the maximum centers of precipitation from the slope of the TP to that of the HM. Along the HM, the contribution of the nonlinear term $-<\omega'\partial_p q'>$ (Fig. 6d) resulting from both vertical motion anomalies and moisture changes is locally significant (> 5 mm day^{-1}), indicating the interaction between the vertical motion and moisture change. In summary, the uplift of the HM increases orographic precipitation and creates the rain shadow effect, with little impacts on the SASM precipitation.

4.2. The thermal effect of the IP

We further explore the responses of the monsoon relevant variables to the uplifts of the IP and HM and the involved physical processes with focus on the effect of the IP. With the IP uplift, the airs of high equivalent potential temperature (θ_e) at lower troposphere are accumulated in the IP and the surrounding region (Fig. 7a), indicating the insulation effect of the uplifted IP (Boos and Kuang, 2010; Acosta and Huber, 2020). Meanwhile, tropical moisture is advected by the anomalous southeasterly from tropical ocean via the Arabian Sea into the northwestern India and Pakistan (Fig. 7b), increasing the tropical convective instability. At 500 hPa, the upward motion anomalies are found over the IP and along the HM (Fig. 7c), reflecting the lifting effect of the elevated topography, which result in the positive thermodynamic term (Fig. 5d). The height of the lifted condensation level (LCL) is significantly reduced over the IP and along the western edge of the HM (Fig. 7d), which is likely resulted from the elevated surface sensible heating (He, 2017). Reduced LCL facilitates the moist convection to occur, further warming the air parcels by the released latent heating. Consequently, specific humidity and θ_e further increase in the middle troposphere (Fig. 7e), which in return favors the convection activity, particularly in the northeastern IP and along the HM where the thermodynamic process caused by humidity change (Fig. 5c) contribute significantly to precipitation change. The pattern match between the specific humidity and θ_e indicates that the increased θ_e is primarily contributed by the humidity increase. At the upper troposphere, forced by the latent heating, the warm-centered South Asian High strengthens over the IP (Fig. 7f), which is coupled with the cyclonic anomaly at low level (Fig. 7b), leading to moisture convergence over the western region and accelerate the convection activity. Positive feedback is thus built between the precipitation and the large-scale circulation.

https://doi.org/10.5194/cp-2022-76
Preprint. Discussion started: 18 November 2022

Climate of the Past
Discussions

We take two grids to illustrate the thermal and dynamical adjustments in vertical structure in response to topographic change. The two grids are located at the west of the HM (wHM, 65°E, 28°N) and the eastern HM (eHM, 80°E, 25°N), which are mainly impacted by the IP and HM uplift, respectively. Both grids show positive and negative vorticity at lower and upper troposphere, respectively, corresponding to the Indian monsoon trough near surface and the South Asia High at upper layer. The wHM grid (Fig. 8a) is located at the southern margin of Asian thermal low where the convergence/divergence structure is not apparent. Ascending movement is relatively shallow and monotonously reduced to 0 in the IP0 experiment at 250 hPa but it remarkably increases at mid-high troposphere to 0.02 Pa s^{-1} when the IP is present (Fig. 8c). At the eHM grid (Fig. 8b), the dynamical structure bears typical deep convection feature, i.e., convergence at lower lever and divergence at high level and strong and deep upward motion (ca 0.04 Pa s^{-1}). The uplift of the HM only weakly strengthens the upward motion at mid-upper level (400-150 hPa).

The diabatic heating acts as an important forcing on the atmosphere circulations (Gill, 1980). The total diabatic heating (TDH) is the sum of the vertical diffusion heating (VH), the latent heating (LH) and radiative heating (RAD). The VH is generally shallow near the surface and the TDH in the free troposphere is determined by LH (Figs. 8c-d). The VH in boundary layer is much larger at wHM than at eHM, indicating stronger surface sensible heating in the western region. With the IP uplift, the TDH at wHM increases from 0.7 to 1.7 K day^{-1} due to enhanced LH, leading to increased air temperature by 0.5 K, which in turn is in favor of convective activity and releases more LH in the free troposphere (Fig. 8c), leading to the large-scale circulation adjustment (Figs. 7b and f). The positive feedback between precipitation and large-scale circulation is thus formed. Whereas at the eHM grid (Fig. 8d), despite the large values of the LH dominated diabatic heating (ca 3K day^{-1}), its change in response to the HM uplift is insignificant, failing to warm air parcels enough to produce monsoon favorable circulation pattern. As a result, only orographic precipitation increases along the windward side.

5. Discussion

5.1. Comparison with previous modeling studies

It is a matter of debate about the effect of the HM and the IP uplift on the intensification of SASM (Boos and Kuang, 2010; Wu et al., 2012; Zhang et al., 2012, 2015; Tang et al., 2013; Acosta and Huber, 2020). Our modeling results confirm the studies which suggested the intensified SASM with the uplift of the IP (Wu et al., 2012; Zhang et al., 2015; Acosta and

Huber, 2020), but we emphasize the intensification mainly over the western region, i.e., from the Arabian Sea to the northwestern India and Pakistan. The uplift of the HM only enhances the orographic precipitation along the windward side of the HM, and has little impact on monsoonal precipitation. In the studies concluding the enhanced SASM attributing to elevated HM (Boos and Kuang, 2010; Zhang et al., 2012), the experiments were potentially supposed that the HM rose to modern height before the presence of elevated TP, which disagrees with the latest geological evidence and the widely held belief (Ding et al., 2017; Wang et al., 2014), the modeling results is thus unsuitable to interpret the paleo-monsoon reconstructions.

Concerning the mechanism of the IP uplift on the SASM, our analyses confirm its thermal forcing effect (Wu et al., 2012; Zhang et al., 2015). Previous studies revealed that the cyclonic circulation results from surface sensible heating (Wu et al., 2012; Liu et al., 2017) and emphasized the sensible heating effect on the SASM. Our analyses reveal that the latent heating is a crucial link between the convection activity and large-scale circulation. Although the importance of the latent heating on the SASM precipitation has been acknowledged by previous study (Zhang et al., 2015), our study provides a more detailed processes and highlights the coupling of the moisture advection with the large-scale circulation, which together intensify the upward motion and the enhanced monsoonal precipitation over the Arabian Sea and the northwestern India. By contrast, despite moist convection and latent heating exist in the case of the HM uplift (Fig. 4c), there is no favorable atmospheric circulation to maintain monsoonal precipitation, only orographic precipitation occurs along the south slope of the HM.

The blocking effect of the IP is also shown in our simulations as the presence of the IP reduces the westerly flow (Fig. 4a) and blocks the cold dry extratropical air from northern India (Fig. 7a). However, we cannot conclude the dominant effect of the mechanical blocking as Tang13 did. In their study, the elevated IP greatly blocked the westerly flow to the south of the HM, facilitating the moisture advection from the Bay of Bengal into northern India, thus strongly enhanced the SASM precipitation, particularly in eastern India. Relatively, the removal of the sensible heating only slightly reduced the SASM precipitation, in contrast with the finding of Wu12 pointing out that the sensible heating strongly enhanced the SASM precipitation. In our study, the elevated IP enhances precipitation in the western India but has little impact in the eastern India. Acosta and Huber (2020) reported that it was the HM that strengthens the easterly moisture flux from the Bay of Bengal into the northern India while the uplifted IP strengthens the moisture flux from the Arabian Sea into northwestern India. The blocking effect of the IP is possibly overestimated by Tang13. However, the two effects cannot

https://doi.org/10.5194/cp-2022-76
Preprint. Discussion started: 18 November 2022

Climate of the Past
Discussions

be separated in nature, we explore the physical processes responsible for the intensification of the SASM in the perspective of the thermal forcing meanwhile acknowledge the importance of the blocking and insulation effect.

5.2. Application to monsoonal reconstructions

Although monsoon-like climate possibly existed at 34 Ma linked to the Proto-TP (Licht et al., 2014), a wide establishment of the SASM at middle Miocene is revealed by increasing evidence (Fig. 3c; Table 1). The inception/intensification of the SASM is asynchronous within the monsoon region. In the western India and over the Arabian Sea, the SASM appeared in the early Miocene (Clift et al., 2008; Reuter et al., 2013; Betzler et al., 2016) and intensified at ~15-12 Ma (Clift et al., 2008; Gupta et al., 2015; Betzler et al., 2016; Zhang et al., 2017), while in the eastern India, the SASM intensification occurred at 14-13 Ma (Khan et al., 2014; Ali et al., 2017; Bhatia et al., 2020). The evolution history of the HM and IP is controversial and has substantial time uncertainty. The latest geology study suggested that HM had against the TP risen to 2.3 ± 0.9 km by earliest Miocene, to ~4 km by 19 Ma, and projected significantly above the average elevation of the plateau from 15 Ma onwards (Ding et al., 2017). The uplift of the IP was thought to occur during the middle-late Miocene (16.5-10.7 Ma) and accelerated after 12.4 Ma (Mouthereau et al., 2011; Khadivi et al.,2012; Ballato et al., 2017), broadly overlapping with the uplifting history of the HM during the middle Miocene.

Our modelling results confirm the appearance of the SASM in early Miocene and agree with a gradual increase in monsoonal precipitation to the west of the Indian landmass during middle Miocene as well as the wide establishment of the SASM in late middle Miocene. But our simulations do not support the interpretation of the monsoon intensification attributed to the HM uplift as some studies did (Clift et al., 2008; Gupta et al., 2015; Betzler et al., 2016; Zhuang et al., 2017). According to our study, it is the uplift of the IP that leads to the strengthening of the SASM in the form of the joint uplift of the IP and the HM. The HM itself has little impacts on the development of the SASM in the western region. The enhanced precipitation at 13 Ma inferred from leaf fossil in the eastern HM is suggested to attribute to the rise of the HM (Bhatia et al., 2021). This monsoon-HM linkage cannot be replicated by our experiments. However, even if the SASM precipitation intensifies during this period, the change in the eastern India is likely subtle. For instance, both the plant fossils and the weathering data indicated that climate in the eastern portion of the HM has stayed rather constant over the last 13 Myr (Khan et al., 2014; Vogeli et al., 2017), suggesting the HM uplift

https://doi.org/10.5194/cp-2022-76
Preprint. Discussion started: 18 November 2022

has little effect on the SASM in eastern India. The uplift of the IP during the middle-late Miocene strengthens the cyclonic circulation over the Arabian Sea, leading to the strengthening of the surface wind (Gupta et al., 2015; Zhuang et al., 2017) and enhanced precipitation over the Arabian Sea (Bialik et al., 2020) as well as in the northwestern India (Clift et al., 2008; Yang et al., 2020). To better understand the evolution of the SASM, more accurate paleo-altimetry studies over the IP including Hindu Kush Mountains would be particularly needed.

In addition to the effect of the IP, modelling studies also suggested the importance of the Eastern African and Arabian topographies in the formation of the SASM (Chakraborty et al., 2006; Wei and Bondoni, 2016; Sarr et al., 2022) although their impacts on the cyclonic circulation and the wind strength in the northern Arabian Sea are less significant (Sarr et al., 2022). Besides, the topographic change is not the only driving forcing that triggered the onset of modern SASM. The expansion of the Antarctic ice sheets from ~14.2 to 13.8 Ma and the final closure of the Tethyan Seaway ~14 Ma likely influenced the oceanic circulations and thus impacted the SASM intensity (Hamon et al., 2013a). Changes of the ice sheet in Antarctic was found to significantly impact the climate in Europe by modifying the oceanic circulation (Hamon et al., 2013b) and the East Asia monsoon through a northward shift of the Intertropical Convergence Zone (Shi et al., 2020), but its impact on the SASM is negligible (Sarr et al., 2022). The intensification of the SASM during the middle Miocene could have been caused by a combination of changes in topography and geography as well as the ocean-atmospheric circulation related to decreasing atmospheric CO_2, changes in orbital forcing, and the progressive cryosphere expansion on Antarctica, which will be addressed in future study.

6. Conclusions

There is increasing evidence of the significant intensification of the SASM during middle Miocene (16-11 Ma). The linkage between large-scale mountains in the TP region and the SASM has long been studied, particularly the HM and the IP that coincidently uplifted during the Miocene. However, their climatic effect on the SASM and the mechanisms are vigorously debated, strongly depending on the geology history of the TP and the surrounding mountains. Many modeling studies have been conducted with a hierarchy of climate models. Most of them are employed AGCMs based on modern geography. With realistic early to middle Miocene paleogeography, we use fully coupled earth system model CESM at relatively highly spatial resolution (~2°) to conduct a series of orographic sensitivity experiments. We examine the effect of elevated IP and HM on the SASM and explore the underlying mechanisms. The conclusions are as follows:

1) The CESM successfully simulates the broad features of the SASM system including the monsoon circulation and precipitation. It also produces the wide establishment of the SASM in middle Miocene, roughly consistent with the reconstructions.
2) We confirm and extend previous studies that the uplift of the IP plays a dominant role in the enhancement of SASM in the western region, i.e., from the northern Arabian Sea to northwestern India and Pakistan, whereas it has little effects in eastern India. The effect of the HM uplift is confined to the range of the HM and its vicinity, producing orographic precipitation change and rain shadow effect. We interpret the intensification of the middle Miocene SASM in the western region as response to the IP uplift while the subtle SASM change in the eastern region reflects the effects of the HM uplift.
3) The uplift of the IP not only insulates the warm and moist air from the westerly in the south of the IP but also produces a low-level cyclonic circulation around the IP, which leads to moisture convergence in the northwestern India and triggers positive feedback between the moist convection and the large-scale monsoon circulation, further increasing the monsoonal precipitation.

Author contribution

MZ and YZ wrote the draft manuscript and analyzed the simulations. YS performed the simulations; GR and TZ modified the draft and particularly corrected the abstract and conclusions. YZ and DL conceived and developed the research. All authors participated in the final version of the manuscript.

Competing interest

The authors declare that they have no conflict of interest.

Acknowledgements

This work is jointly supported by the Second Tibetan Plateau Scientific Expedition and Research Program (STEP; Grant No. 2019QZKK0708) and the National Natural Science Foundation of China (Grants 41988101, 42105047). Model simulations presented in this study were performed on the supercomputer of Chinese Academy of Science Jin Cloud.

https://doi.org/10.5194/cp-2022-76
Preprint. Discussion started: 18 November 2022

References

Acosta, R.P., Huber, M., 2020. Competing Topographic Mechanisms for the Summer Indo-Asian Monsoon. Geophysical Research Letters 47, e2019GL085112. https://doi.org/10.1029/2019GL085112

Ali, S., E. C. Hathorne, and M. Frank, 2021: Persistent provenance of south asian monsoon-induced silicate weathering over the past 27 million years. Paleoceanography and Paleoclimatology, 36, https://doi.org/10.1029/2020pa003909.

Anand, A., Mishra, S.K., Sahany, S., Bhowmick, M., Rawat, J.S., Dash, S.K., 2018. Indian Summer Monsoon Simulations: Usefulness of Increasing Horizontal Resolution, Manual Tuning, and Semi-Automatic Tuning in Reducing Present-Day Model Biases. Sci Rep 8, 3522. https://doi.org/10.1038/s41598-018-21865-1

An, Z. S., J. E. Kutzbach, W. L. Prell, and S. C. Porter, 2001: Evolution of asian monsoons and phased uplift of the himalayan tibetan plateau since late miocene times. Nature, 411, 62-66, https://doi.org/10.1038/35075035.

Ballato, P., Cifelli, F., Heidarzadeh, G., Ghassemi, M.R., Wickert, A.D., Hassanzadeh, J., Dupont-Nivet, G., Balling, P., Sudo, M., Zeilinger, G., Schmitt, A.K., Mattei, M., Strecker, M.R., 2017. Tectono-sedimentary evolution of the northern Iranian Plateau: insights from middle–late Miocene foreland-basin deposits. Basin Research 29, 417–446. https://doi.org/10.1111/bre.12180

Betzler, C., and Coauthors, 2016: The abrupt onset of the modern south asian monsoon winds. Sci. Rep., 6, https://doi.org/10.1038/srep29838.

Bhatia, H., Srivastava, G., Spicer, R.A., Farnsworth, A., Spicer, T.E.V., Mehrotra, R.C., Paudayal, K.N., Valdes, P., 2021. Leaf physiognomy records the Miocene intensification of the South Asia Monsoon. Global and Planetary Change 196, 103365. https://doi.org/10.1016/j.gloplacha.2020.103365

Bialik, O. M., G. Auer, N. O. Ogawa, D. Kroon, N. D. Waldmann, and N. Ohkouchi, 2020: Monsoons, upwelling, and the deoxygenation of the northwestern indian ocean in response to middle to late miocene global climatic shifts. Paleoceanography and Paleoclimatology, 35, https://doi.org/10.1029/2019pa003762.

Boos, W., Kuang, Z., 2010. Dominant control of the South Asian Monsoon by orographic insulation versus plateau heating. Nature 463, 218–22. https://doi.org/10.1038/nature08707

Bosboom, R., Dupont-Nivet, G., Grothe, A., Brinkhuis, H., Villa, G., Mandic, O., Stoica, M., Kouwenhoven, T., Huang, W., Yang, W., Guo, Z., 2014. Timing, cause and impact of the late Eocene stepwise sea retreat from the Tarim Basin (west China). Palaeogeography, Palaeoclimatology, Palaeoecology 403, 101–118. https://doi.org/10.1016/j.palaeo.2014.03.035

Botsyun, S., P. Sepulchre, Y. Donnadieu, C. Risi, A. Licht, and J. K. C. Rugenstein, 2019: Revised paleoaltimetry data show low tibetan plateau elevation during the eocene. Science, 363, 946-+, https://doi.org/10.1126/science.aaq1436.

Burg, J.P., Chen, G.M., 1984. Tectonics and structural zonation of southern Tibet, China. Nature 311, 219–223. https://doi.org/10.1038/311219a0

Burls, N.J., Bradshaw, C.D., Boer, A.M.D., Herold, N., Huber, M., Pound, M., Donnadieu, Y., Farnsworth, A., Frigola, A., Gasson, E., Heydt, A.S. von der, Hutchinson, D.K., Knorr, G., Lawrence, K.T., Lear, C.H., Li, X., Lohmann, G., Lunt, D.J., Marzocchi, A., Prange, M., Riihimaki, C.A., Sarr, A.-C., Siler, N., Zhang, Z., 2021. Simulating Miocene Warmth: Insights From an Opportunistic Multi-Model Ensemble (MioMIP1). Paleoceanography and Paleoclimatology 36, e2020PA004054. https://doi.org/10.1029/2020PA004054

Chakraborty, A., Nanjundiah, R.S., Srinivasan, J., 2006. Theoretical aspects of the onset of

Indian summer monsoon from perturbed orography simulations in a GCM. Annales Geophysicae 24, 2075–2089.

Chen, X., and T. Zhou, 2015: Distinct effects of global mean warming and regional sea surface warming pattern on projected uncertainty in the south asian summer monsoon. Geophys. Res. Lett., 42, 9433-9439, https://doi.org/10.1002/2015gl066384.

Chen, G.-S., Liu, Z., Kutzbach, J., 2014. Reexamining the barrier effect of the Tibetan Plateau on the South Asian summer monsoon. Climate of the Past 10. https://doi.org/10.5194/cp-10-1269-2014

Chou, C., J. D. Neelin, C.-A. Chen, and J.-Y. Tu, 2009: Evaluating the "rich-get-richer" mechanism in tropical precipitation change under global warming. J. Climate, 22, 1982-2005, https://doi.org/10.1175/2008jcli2471.1.

Clift, P.D., Hodges, K.V., Heslop, D., Hannigan, R., Van Long, H., Calves, G., 2008. Correlation of Himalayan exhumation rates and Asian monsoon intensity. Nature Geosci 1, 875–880. https://doi.org/10.1038/ngeo351

Clift, P.D., Webb, A.A.G., 2019. A history of the Asian monsoon and its interactions with solid Earth tectonics in Cenozoic South Asia. Geological Society, London, Special Publications 483, 631–652. https://doi.org/10.1144/SP483.1

Ding, L., Spicer, R.A., Yang, J., Xu, Q., Cai, F., Li, S., Lai, Q., Wang, H., Spicer, T.E.V., Yue, Y., Shukla, A., Srivastava, G., Khan, M.A., Bera, S., Mehrotra, R., 2017. Quantifying the rise of the Himalaya orogen and implications for the South Asian monsoon. Geology 45, 215–218. https://doi.org/10.1130/G38583.1

Ding, L., P. Kapp, F. Cai, C. N. Garzione, Z. Xiong, H. Wang, and C. Wang, 2022: Timing and mechanisms of tibetan plateau uplift. Nature Reviews Earth & Environment, https://doi.org/10.1038/s43017-022-00318-4.

ECMWF, 2017. Copernicus Climate Change Service: ERA5: Fifth generation of ECMWF atmospheric reanalyses of the global climate. Copernicus Climate Change Service Climate Data Store (CDS) [WWW Document]. ECMWF. URL https://www.ecmwf.int/en/about/what-we-do/environmental-services/copernicus-climate-change-service (accessed 11.5.21).

England, P., Houseman, G., 1989. Extension during continental convergence, with application to the Tibetan Plateau. https://doi.org/10.1029/JB094IB12P17561

Eyring, V., Bony, S., Meehl, G.A., Senior, C.A., Stevens, B., Stouffer, R.J., Taylor, K.E., 2016. Overview of the Coupled Model Intercomparison Project Phase 6 (CMIP6) experimental design and organization. Geoscientific Model Development 9, 1937–1958. https://doi.org/10.5194/gmd-9-1937-2016

Farnsworth, A., Lunt, D.J., Robinson, S.A., Valdes, P.J., Roberts, W.H.G., Clift, P.D., Markwick, P., Su, T., Wrobel, N., Bragg, F., Kelland, S.-J., Pancost, R.D., 2019. Past East Asian monsoon evolution controlled by paleogeography, not CO2. Science Advances 5, eaax1697. https://doi.org/10.1126/sciadv.aax1697

Favre, A., Päckert, M., Pauls, S.U., Jähnig, S.C., Uhl, D., Michalak, I., Muellner-Riehl, A.N., 2015. The role of the uplift of the Qinghai-Tibetan Plateau for the evolution of Tibetan biotas. Biological Reviews 90, 236–253. https://doi.org/10.1111/brv.12107

Fluteau, F., Ramstein, G., Besse, J., 1999. Simulating the evolution of the Asian and African monsoons during the past 30 Myr using an atmospheric general circulation model. Journal of Geophysical Research: Atmospheres 104, 11995–12018. https://doi.org/10.1029/1999JD900048

Frigola, A., Prange, M., Schulz, M., 2018. Boundary conditions for the Middle Miocene Climate Transition (MMCT v1. 0). Geoscientific Model Development 11, 1607–1626.

Gadgil, S., M. Rajeevan, and R. Nanjundiah, 2005: Monsoon prediction - why yet another failure? Current Science, 88, 1389-1400.

https://doi.org/10.5194/cp-2022-76
Preprint. Discussion started: 18 November 2022

Gébelin, A., Mulch, A., Teyssier, C., Jessup, M.J., Law, R.D., Brunel, M., 2013. The Miocene elevation of Mount Everest. Geology 41, 799–802. https://doi.org/10.1130/G34331.1

Gent, P.R., Danabasoglu, G., Donner, L.J., Holland, M.M., Hunke, E.C., Jayne, S.R., Lawrence, D.M., Neale, R.B., Rasch, P.J., Vertenstein, M., Worley, P.H., Yang, Z.-L., Zhang, M., 2011. The Community Climate System Model Version 4. Journal of Climate 24, 4973–4991. https://doi.org/10.1175/2011JCLI4083.1

Gill, A.E., 1980. Some simple solutions for heat-induced tropical circulation. Q.J Royal Met. Soc. 106, 447–462. https://doi.org/10.1002/qj.49710644905

Goldner, A., Herold, N., Huber, M., 2014. The Challenge of Simulating the Warmth of the Mid-Miocene Climatic Optimun in CESM1. Climate of the Past.

Guo, Z.T., Sun, B., Zhang, Z.S., Peng, S.Z., Xiao, G.Q., Ge, J.Y., Hao, Q.Z., Qiao, Y.S., Liang, M.Y., Liu, J.F., Yin, Q.Z., Wei, J.J., 2008. A major reorganization of Asian climate by the early Miocene. Climate of the Past 4, 153–174. https://doi.org/10.5194/cp-4-153-2008

Gupta, A. K., A. Yuvaraja, M. Prakasam, S. C. Clemens, and A. Velu, 2015: Evolution of the south asian monsoon wind system since the late middle miocene. Palaeogeography Palaeoclimatology Palaeoecology, 438, 160-167, https://doi.org/10.1016/j.palaeo.2015.08.006.

Hamon, N., Sepulchre, P., Lefebvre, V., Ramstein, G., 2013. The role of eastern Tethys seaway closure in the Middle Miocene Climatic Transition (ca. 14 Ma). Climate of the Past 9, 2687–2702. https://doi.org/10.5194/cp-9-2687-2013

Hamon, N., P. Sepulchre, Y. Donnadieu, A. J. Henrot, L. Francois, J. J. Jaeger, and G. Ramstein, 2012: Growth of subtropical forests in miocene europe: The roles of carbon dioxide and antarctic ice volume. Geology, 40, 567-570, https://doi.org/10.1130/g32990.1.

Harris, N., 2006. The elevation history of the Tibetan Plateau and its implications for the Asian monsoon. Palaeogeography, Palaeoclimatology, Palaeoecology, Monsoon and Tectonics of Asia 241, 4–15. https://doi.org/10.1016/j.palaeo.2006.07.009

He, B., 2017. Influences of elevated heating effect by the Himalaya on the changes in Asian summer monsoon. Theor Appl Climatol 128, 905–917. https://doi.org/10.1007/s00704-016-1746-5

Herold, N., M. Seton, R. D. Mueller, Y. You, and M. Huber, 2008: Middle miocene tectonic boundary conditions for use in climate models. Geochemistry Geophysics Geosystems, 9, https://doi.org/10.1029/2008gc002046.

Herold, N., M. Huber, and R. D. Mueller, 2011: Modeling the miocene climatic optimum. Part i: Land and atmosphere. J. Climate, 24, 6353-6372, https://doi.org/10.1175/2011jcli4035.1.

Herold, N., M. Huber, R. D. Mueller, and M. Seton, 2012: Modeling the miocene climatic optimum: Ocean circulation. Paleoceanography, 27, https://doi.org/10.1029/2010pa002041.

Hersbach, H., and Coauthors, 2020: The era5 global reanalysis. Quarterly Journal of the Royal Meteorological Society, 146, 1999-2049, https://doi.org/10.1002/qj.3803.

Huffman, G. J., R. F. Adler, D. T. Bolvin, and G. Gu, 2009: Improving the global precipitation record: Gpcp version 2.1. Geophys. Res. Lett., 36, https://doi.org/10.1029/2009gl040000.

Hunke, E.C., Lipscomb, W.H., 2010. CICE: the Los Alamos Sea Ice Model Documentation and Software User's Manual Version 4. 1–76.

Jin, C., B. Wang, and J. Liu, 2020: Future changes and controlling factors of the eight regional monsoons projected by cmip6 models. J. Climate, 33, 9307-9326, https://doi.org/10.1175/jcli-d-20-0236.1.

Khan, M.A., Spicer, R.A., Bera, S., Ghosh, R., Yang, J., Spicer, T.E.V., Guo, S., Su, T., Jacques, F., Grote, P.J., 2014. Miocene to Pleistocene floras and climate of the Eastern Himalayan Siwaliks, and new palaeoelevation estimates for the Namling–Oiyug Basin, Tibet. Global and Planetary Change 113, 1–10. https://doi.org/10.1016/j.gloplacha.2013.12.003

https://doi.org/10.5194/cp-2022-76
Preprint. Discussion started: 18 November 2022

Kitoh, A., 2002. Effects of Large-Scale Mountains on Surface Climate. A Coupled Ocean-Atmosphere General Circulation Model Study. Journal of the Meteorological Society of Japan 80, 1165–1181. https://doi.org/10.2151/jmsj.80.1165

Kitoh, A., 2017: The asian monsoon and its future change in climate models: A review. Journal of the Meteorological Society of Japan, 95, 7-33, https://doi.org/10.2151/jmsj.2017-002.

Krapp, M., and J. H. Jungclaus, 2011: The middle miocene climate as modelled in an atmosphere-ocean-biosphere model. Climate Past, 7, 1169-1188, https://doi.org/10.5194/cp-7-1169-2011.

Kutzbach, J.E., Guetter, P.J., Ruddiman, W.F., Prell, W.L., 1989. Sensitivity of climate to late Cenozoic uplift in southern Asia and the American west: Numerical experiments. Journal of Geophysical Research: Atmospheres 94, 18393–18407. https://doi.org/10.1029/JD094iD15p18393

Licht, A., and Coauthors, 2014: Asian monsoons in a late eocene greenhouse world. Nature, 513, 501-506, https://doi.org/10.1038/nature13704.

Li, S.-F., and Coauthors, 2021: Orographic evolution of northern tibet shaped vegetation and plant diversity in eastern asia. Science Advances, 7, https://doi.org/10.1126/sciadv.abc7741.

Liu, G., Li-Ren, J., Sun, S.-Q., Xin, Y.-F., 2012. Low- and Mid-High Latitude Components of the East Asian Winter Monsoon and Their Reflecting Variations in Winter Climate over Eastern China. Atmospheric and Oceanic Science Letters 5, 195–200. https://doi.org/10.1080/16742834.2012.11446985

Liu, X., and B. Dong, 2013: Influence of the tibetan plateau uplift on the asian monsoon-arid environment evolution. Chinese Science Bulletin, 58, 4277-4291, https://doi.org/10.1007/s11434-013-5987-8.

Liu, X., Xu, Q., Ding, L., 2016. Differential surface uplift: Cenozoic paleoelevation history of the Tibetan Plateau. Sci. China Earth Sci. 59, 2105–2120. https://doi.org/10.1007/s11430-015-5486-y

Liu, X., Yin, Z.-Y., 2002. Sensitivity of East Asian monsoon climate to the uplift of the Tibetan Plateau. Palaeogeography, Palaeoclimatology, Palaeoecology 3–4, 223–245.

Liu, Y., Wang, Z., Zhuo, H., Wu, G., 2017. Two types of summertime heating over Asian large-scale orography and excitation of potential-vorticity forcing II. Sensible heating over Tibetan-Iranian Plateau. Sci. China Earth Sci. 60, 733–744. https://doi.org/10.1007/s11430-016-9016-3

Lunt, D.J., Flecker, R., Clift, P.D., 2010. The impacts of Tibetan uplift on palaeoclimate proxies. Geological Society, London, Special Publications 342, 279–291. https://doi.org/10.1144/SP342.16

Ma, D., Boos, W., Kuang, Z., 2014. Effects of Orography and Surface Heat Fluxes on the South Asian Summer Monsoon. Journal of Climate 27, 6647–6659. https://doi.org/10.1175/JCLI-D-14-00138.1

Manabe, S., Terpstra, T.B., 1974. The Effects of Mountains on the General Circulation of the Atmosphere as Identified by Numerical Experiments. Journal of the Atmospheric Sciences 31, 3–42. https://doi.org/10.1175/1520-0469(1974)031<0003:TEOMOT>2.0.CO;2

McQuarrie, N., Stock, J.M., Verdel, C., Wernicke, B.P., 2003. Cenozoic evolution of Neotethys and implications for the causes of plate motions. Geophysical Research Letters 30. https://doi.org/10.1029/2003GL017992

Morley, R.J., 2007. Cretaceous and Tertiary climate change and the past distribution of megathermal rainforests, in: Bush, M.B., Flenley, J.R. (Eds.), Tropical Rainforest Responses to Climatic Change, Springer Praxis Books. Springer, Berlin, Heidelberg, pp. 1–31. https://doi.org/10.1007/978-3-540-48842-2_1

Mouthereau, F., 2011. Timing of uplift in the Zagros belt/Iranian plateau and accommodation

https://doi.org/10.5194/cp-2022-76
Preprint. Discussion started: 18 November 2022

of late Cenozoic Arabia–Eurasia convergence. Geological Magazine 148, 726–738. https://doi.org/10.1017/S0016756811000306

Neale, R.B., Richter, J., Park, S., Lauritzen, P.H., Vavrus, S.J., Rasch, P.J., Zhang, M., 2013. The Mean Climate of the Community Atmosphere Model (CAM4) in Forced SST and Fully Coupled Experiments. Journal of Climate 26, 5150–5168. https://doi.org/10.1175/JCLI-D-12-00236.1

O'Brien, T. A., and Coauthors, 2013: Observed scaling in clouds and precipitation and scale incognizance in regional to global atmospheric models. Journal of climate, 26, 9313-9333, https://doi.org/10.1175/jcli-d-13-00005.1.

Pound, M.J., Haywood, A.M., Salzmann, U., Riding, J.B., 2012. Global vegetation dynamics and latitudinal temperature gradients during the Mid to Late Miocene (15.97–5.33Ma). Earth-Science Reviews 112, 1–22. https://doi.org/10.1016/j.earscirev.2012.02.005

Prell, W. L., and J. E. Kutzbach, 1992: Sensitivity of the indian monsoon to forcing parameters and implications for its evolution. Nature, 360, 647-652, https://doi.org/10.1038/360647a0.

Quade, J., Cerling, T.E., Bowman, J.R., 1989. Development of Asian monsoon revealed by marked ecological shift during the latest Miocene in northern Pakistan. Nature 342, 163–166. https://doi.org/10.1038/342163a0

Ramage, C. (1971), Monsoon Meteorology,Int. Geophys. Ser., vol. 15, 296 pp., Academic Press, San Diego, Cali.

Ramstein, G., Fluteau, F., Besse, J., Joussaume, S., 1997. Effect of orogeny, plate motion and land-sea distribution on Eurasian climate change over the past 30 million years. Effect of orogeny, plate motion and land-sea distribution on Eurasian climate change over the past 30 million years 386, 788–795.

Rao, Y.P., 1976: Southwest monsoon India Meteorological Department. Meteorological Monograph Synoptic Meteorology, No.1/1976, Delhi, 367 pp.

Reuter, M., W. E. Piller, M. Harzhauser, and A. Kroh, 2013: Cyclone trends constrain monsoon variability during late oligocene sea level highstands (kachchh basin, nw india). Climate Past, 9, 2101-2115, https://doi.org/10.5194/cp-9-2101-2013.

Sarr, A.-C., and Coauthors, 2022: Neogene south asian monsoon rainfall and wind histories diverged due to topographic effects. Nat Geosci, 15, 314-+, https://doi.org/10.1038/s41561-022-00919-0.

Smith, R., P. Jones, B. Briegleb, F. Bryan, and S. Yeager, 2010: The parallel ocean program (pop) reference manual: Ocean component of the community climate system model (ccsm).

Srivastava, G., K. N. Paudayal, T. Utescher, and R. C. Mehrotra, 2018: Miocene vegetation shift and climate change: Evidence from the siwalik of nepal. Global and Planetary Change, 161, 108-120, https://doi.org/10.1016/j.gloplacha.2017.12.001.

Steinthorsdottir, M., Coxall, H., De Boer, A., Huber, M., Barbolini, N., Bradshaw, C., Burls, N., Feakins, S., Gasson, E., Henderiks, J., Holbourn, A.E., Kiel, S., Kohn, M., Knorr, G., Kürschner, W.M., Lear, C.H., Liebrand, D., Lunt, D.J., Mörs, T., Pearson, P., Pound, M.J., Stoll, H., Stromberg, C., 2021. The Miocene: The Future of the Past. Paleoceanography and Paleoclimatology 36. https://doi.org/10.1029/2020PA004037

Su, B., Jiang, D., Zhang, R., Sepulchre, P., Ramstein, G., 2018. Difference between the North Atlantic and Pacific meridional overturning circulation in response to the uplift of the Tibetan Plateau. Climate of the Past 14, 751–762. https://doi.org/10.5194/cp-14-751-2018

Sun, J., Sheykh, M., Ahmadi, N., Cao, M., Zhang, Z., Tian, S., Sha, J., Jian, Z., Windley, B.F., Talebian, M., 2021. Permanent closure of the Tethyan Seaway in the northwestern Iranian Plateau driven by cyclic sea-level fluctuations in the late Middle Miocene. Palaeogeography, Palaeoclimatology, Palaeoecology 564, 110172. https://doi.org/10.1016/j.palaeo.2020.110172

Sundaram, S., Q. Z. Yin, A. Berger, and H. Muri, 2012: Impact of ice sheet induced north atlantic oscillation on east asian summer monsoon during an interglacial 500,000 years ago. Climate Dyn., 39, 1093-1105, https://doi.org/10.1007/s00382-011-1213-z.

Tada, R., H. Zheng, and P. D. Clift, 2016: Evolution and variability of the asian monsoon and its potential linkage with uplift of the himalaya and tibetan plateau. Progress in Earth and Planetary Science, 3, https://doi.org/10.1186/s40645-016-0080-y.

Tang, H., Micheels, A., Eronen, J.T., Ahrens, B., Fortelius, M., 2013. Asynchronous responses of East Asian and Indian summer monsoons to mountain uplift shown by regional climate modelling experiments. Clim Dyn 40, 1531–1549. https://doi.org/10.1007/s00382-012-1603-x

Tardif, D., and Coauthors, 2020: The origin of asian monsoons: A modelling perspective. Climate of the Past, 16, 847-865, https://doi.org/10.5194/cp-16-847-2020.

Turner, A. G., and H. Annamalai, 2012: Climate change and the South Asian summer monsoon. Nature Climate Change, 2, 587-595, https://doi.org/10.1038/nclimate1495.

Vogeli, N., P. Huyghe, P. van der Beek, Y. Najman, E. Garzanti, and C. Chauvel, 2018: Weathering regimein the eastern himalaya since the mid-miocene: Indications fromdetrital geochemistry and claymineralogy of the kameng river section, arunachal pradesh, india. Basin Research, 30, 59-74, https://doi.org/10.1111/bre.12242.

Wang, C., Dai, J., Zhao, X., Li, Y., Graham, S.A., He, D., Ran, B., Meng, J., 2014. Outward-growth of the Tibetan Plateau during the Cenozoic: A review. Tectonophysics 621, 1–43. https://doi.org/10.1016/j.tecto.2014.01.036

Wang, Z., Duan, A., Yang, S., 2019. Potential regulation on the climatic effect of Tibetan Plateau heating by tropical air–sea coupling in regional models. Clim Dyn 52, 1685–1694. https://doi.org/10.1007/s00382-018-4218-z

Wu, G., Liu, Y., He, B., Bao, Q., Duan, A., Jin, F.-F., 2012. Thermal Controls on the Asian Summer Monsoon. Scientific Reports 2, 404. https://doi.org/10.1038/srep00404

Wu, G., Liu, Y., Zhang, Q., Duan, A., Wang, T., Wan, R., Liu, X., Li, W., Wang, Z., Liang, X., 2007. The Influence of Mechanical and Thermal Forcing by the Tibetan Plateau on Asian Climate. Journal of Hydrometeorology 8, 770–789. https://doi.org/10.1175/JHM609.1

Yanai, M., Li, C., 1994. Mechanism of Heating and the Boundary Layer over the Tibetan Plateau. Monthly Weather Review 122, 305–323. https://doi.org/10.1175/1520-0493(1994)122<0305:MOHATB>2.0.CO;2

Yang, H., Wen, Q., 2020. Investigating the Role of the Tibetan Plateau in the Formation of Atlantic Meridional Overturning Circulation. Journal of Climate 33, 3585–3601. https://doi.org/10.1175/JCLI-D-19-0205.1

Yang, X., Groeneveld, J., Jian, Z., Steinke, S., Giosan, L., 2020. Middle Miocene Intensification of South Asian Monsoonal Rainfall. Paleoceanography and Paleoclimatology 35, e2020PA003853. https://doi.org/10.1029/2020PA003853

Zhang, R., Jiang, D., Liu, X., Tian, Z., 2012. Modeling the climate effects of different subregional uplifts within the Himalaya-Tibetan Plateau on Asian summer monsoon evolution. Chin. Sci. Bull. 57, 4617–4626. https://doi.org/10.1007/s11434-012-5284-y

Zhang, R., Jiang, D., Zhang, Z., 2019. Vegetation and Ocean Feedbacks on the Asian Climate Response to the Uplift of the Tibetan Plateau. Journal of Geophysical Research: Atmospheres 124, 6327–6341. https://doi.org/10.1029/2019JD030503

Zhang, R., Jiang, D., Zhang, Z., Yu, E., 2015. The impact of regional uplift of the Tibetan Plateau on the Asian monsoon climate. Palaeogeography, Palaeoclimatology, Palaeoecology 417, 137–150. https://doi.org/10.1016/j.palaeo.2014.10.030

Zhang, R., D. Jiang, Z. Zhang, and C. Zhang, 2021: Effects of tibetan plateau growth, paratethys sea retreat and global cooling on the east asian climate by the early miocene. Geochemistry Geophysics Geosystems, 22, https://doi.org/10.1029/2021gc009655.

Zheng, F., Yuan, Y., Ding, Y., Li, K., Fang, X., Zhao, Y., Sun, Y., Zhu, J., Ke, Z., Wang, J.,

https://doi.org/10.5194/cp-2022-76
Preprint. Discussion started: 18 November 2022

Jia, X., 2021. The 2020/21 Extremely Cold Winter in China Influenced by the Synergistic Effect of La Niña and Warm Arctic. Adv. Atmos. Sci. https://doi.org/10.1007/s00376-021-1033-y

Zhisheng, A., Kutzbach, J.E., Prell, W.L., Porter, S.C., 2001. Evolution of Asian monsoons and phased uplift of the Himalaya–Tibetan plateau since Late Miocene times. Nature 411, 62–66. https://doi.org/10.1038/35075035

Zhuang, G., Pagani, M., Zhang, Y.G., 2017. Monsoonal upwelling in the western Arabian Sea since the middle Miocene. Geology 45, 655–658. https://doi.org/10.1130/G39013.1

https://doi.org/10.5194/cp-2022-76
Preprint. Discussion started: 18 November 2022

Table 1. Evidences of modern SAM in middle Miocene from recently published studies.

No	station	Location (lat/lon)	sample	Intensification age (Ma)	Trend	variable	references
1	Well Indus Marine A-1	24/66	weathering	25-15	decreasing	Precip	Clift et al., 2008
2	ODP 359	5/73	deposit	(25-12.9) 12.9	increasing	wind	Betzler et al., 2016
3	ODP 722B	16.6/59.8	Bio-marker	12.9	increasing	wind	Gupta et al., 2015
	ODP 722B	16.6/59.8	Bio-marker	11	increasing	wind	Zhuang et al., 2017
	ODP 722B	16.6/59.8	Bio-marker	14	increasing	Precip	Bialik et al., 2020
4	NGHP-01-01A	15/71	Bio-marker	(16-11) 14	increasing	Precip	Yang et al., 2020
5	Varkala	8.7/76.7	Pollen fossil	17-15	No change	Precip.	Reuter et al., 2013
6	ODP 758	5.4/90.4	weathering	13.9	increasing	Precip	Ali et al., 2017
7	Surai Khola	27.8/83	Leaf Fossil	13	increasing	Precip.	Srivastava et al., 2018 Bhatia et al., 2021
8	Darjeeling	27/88.5	Leaf Fossil	13	increasing	Precip.	Khan et al., 2014
9	Arunachal Pradesh	27/93.5	Leaf Fossil	13	No change	Precip.	Khan et al., 2014
	Arunachal Pradesh	26/93.5	weathering	13	No change	Precip.	Vogeli et al., 2017

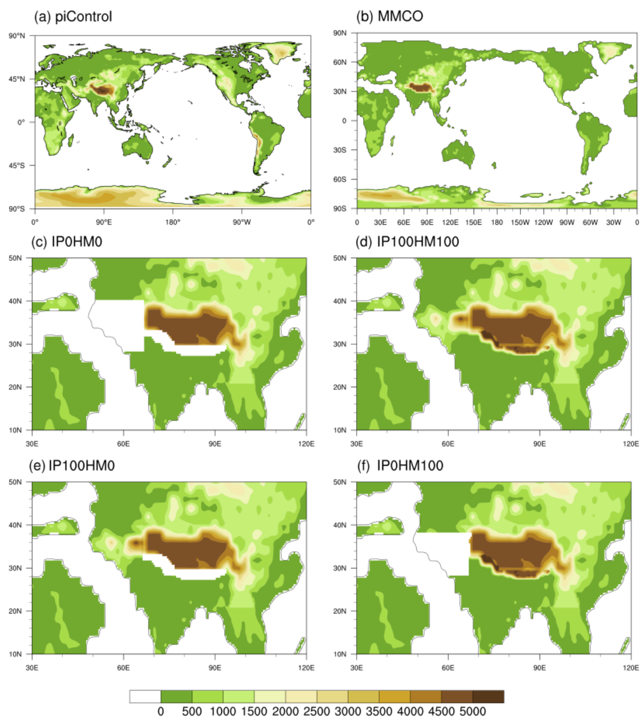

Figure 1. Topography of (a) piControl, (b) MMIO and orographic sensitivity experiments, including (c) IP0HM0, (d) IP100HM100, (e) IP100HM0 and (f) IP0HM100.

https://doi.org/10.5194/cp-2022-76
Preprint. Discussion started: 18 November 2022

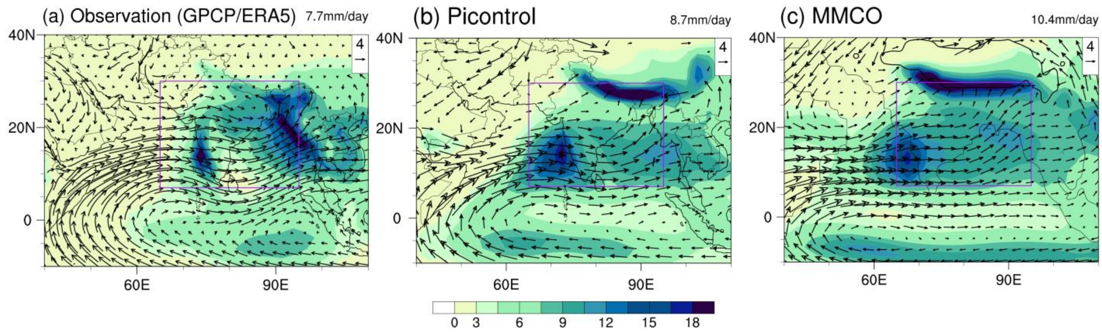

Figure 2. Climatology of JJA (June-July-August) seasonal mean South Asia summer monsoon (SASM) precipitation (mm day^{-1}) and 850 hPa winds (vectors, m s^{-1}) from (a) observation precipitation from GPCP and circulation from ERA5), (b) Preindustrial control experiment and (c) MMIO experiment. Climatology is the average over 1979-2005 for the observation. As for the piControl and MMIO experiment, we select the last 50 and 100 years of simulation, respectively. All Indian rainfall (AIR) is shown at the top-right of each panel. AIR indicates precipitation over the land points within the purple square in each panel (7-30°N, 65-95°E). The black contour in panel c indicates the altitude of 2500 m.

https://doi.org/10.5194/cp-2022-76
Preprint. Discussion started: 18 November 2022

Climate of the Past Discussions

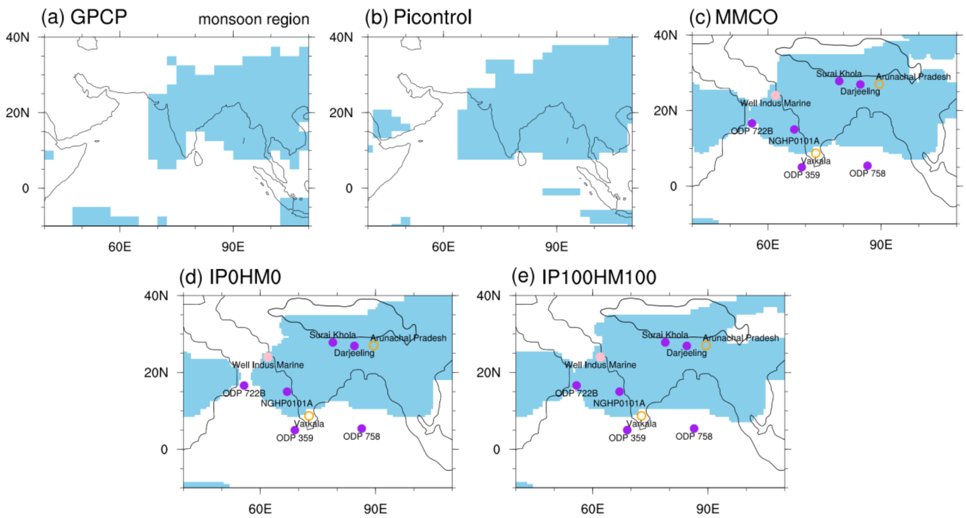

Figure 3. The monsoon domains (blue shading) in (a) GPCP, (b) piControl experiment and (c) MMIO experiment, which are defined by the regions where local summer-minus-winter precipitation exceeds 2 mm day^{-1} and the local summer precipitation exceeds 55% of the annual total. Dots in (c-e) represent reconstructions near the SASM region, purple solid dots denote enhanced SAM, orange circles denote no significant change and pink solid dots denote weakened SAM. The black contour in (c-e) indicates the altitude of 2500 m.

https://doi.org/10.5194/cp-2022-76
Preprint. Discussion started: 18 November 2022

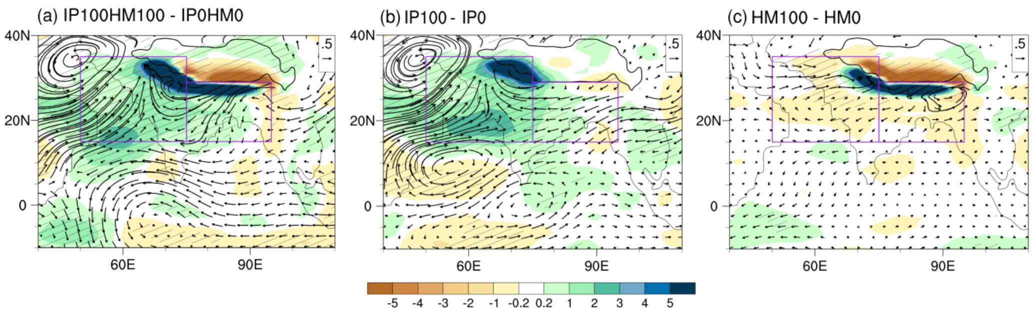

Figure 4. Precipitation (shaded, mm day^{-1}) and 850hPa wind differences between (a) IP100HM100 and IP0HM0 experiments; (b) IP100 IP0 experiments; (c) HM100 and HM0 experiments. The black contour in each panel indicates the altitude of 2500 m. Purple boxes represent west (15-35°N, 50-75°E) and east (15-29°N, 75-95°E) parts of the South Asian monsoon region. Slashes indicate values >95% confidence level based on the *Student's t* test.

https://doi.org/10.5194/cp-2022-76
Preprint. Discussion started: 18 November 2022

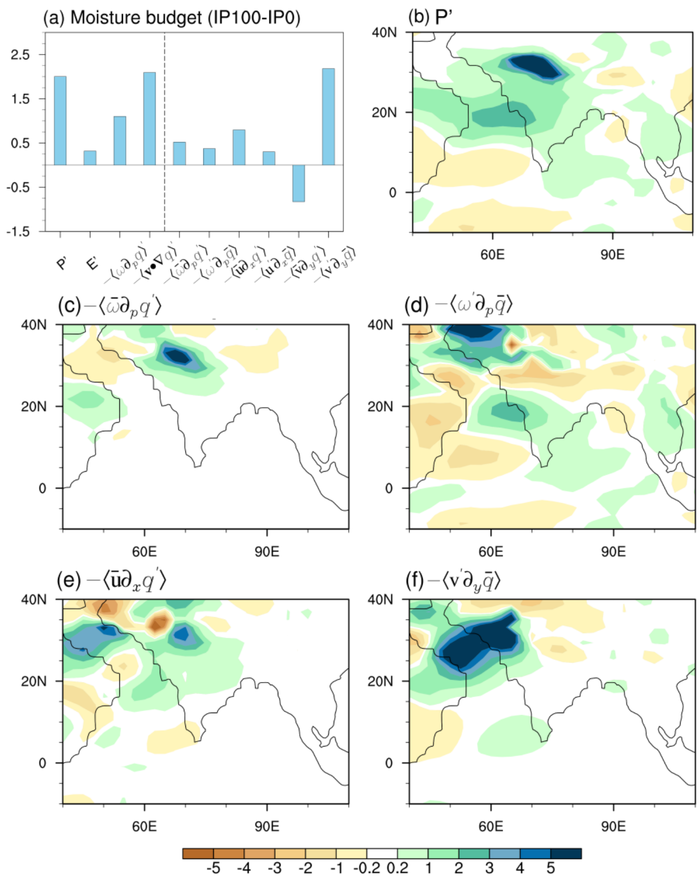

Figure 5. (a) Moisture budget for regional mean precipitation differences (mm day^{-1}) over the west part (15-35°N, 50-75°E) of the South Asian monsoon region between IP100 and IP0 experiments. Spatial distribution of (b) precipitation difference, (c) anomalous vertical moisture advection by climatological vertical motion (thermodynamic term) $-<\overline{\omega}\partial_p q'>$; (d) anomalous advection of the climatological vertical moisture by vertical motion anomalies (dynamic term) $-<\omega'\partial_p\overline{q}>$; (e) anomalous horizontal moisture advection by climatological zonal wind $-<\overline{u}\partial_x q'>$and (f) anomalous horizontal advection of the climatological moisture by meridional wind anomalies $-<v'\partial_y\overline{q}>$.

https://doi.org/10.5194/cp-2022-76
Preprint. Discussion started: 18 November 2022

Climate of the Past Discussions

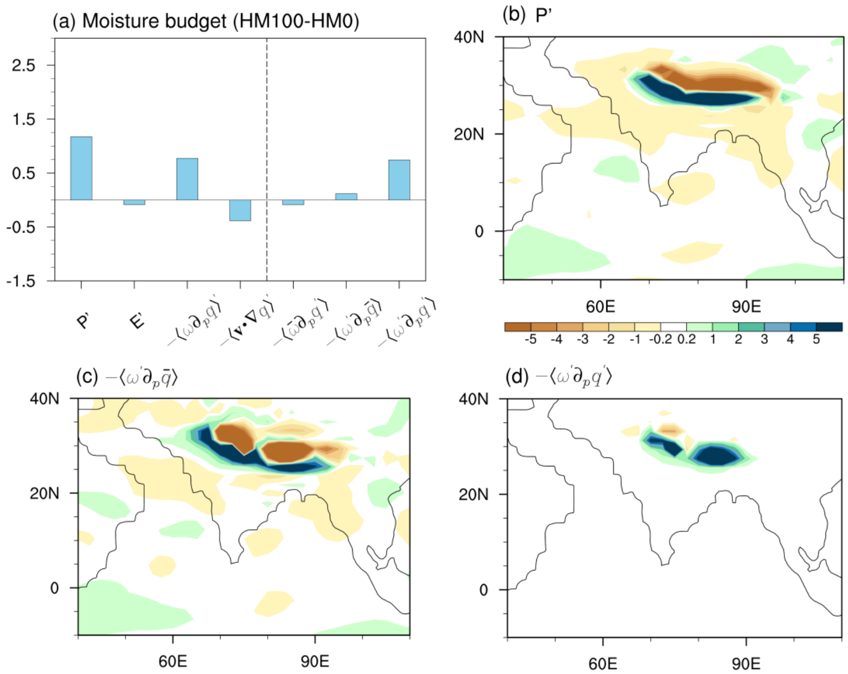

Figure 6. (a) Moisture budget for regional mean precipitation differences (mm day^{-1}) over the east part (15-29°N, 75-95°E) of the South Asian monsoon region between HM100 and HM0 experiments. Spatial distribution of (b) precipitation difference, (c) anomalous advection of the climatological vertical moisture by vertical motion anomalies (dynamic term) $-<\omega'\partial_p\overline{q}>$ and (d) anomalous moisture advection by both vertical motion anomalies and specific humidity anomalies (nonlinear term) $-<\omega'\partial_p q'>$.

https://doi.org/10.5194/cp-2022-76
Preprint. Discussion started: 18 November 2022

Climate of the Past
Discussions

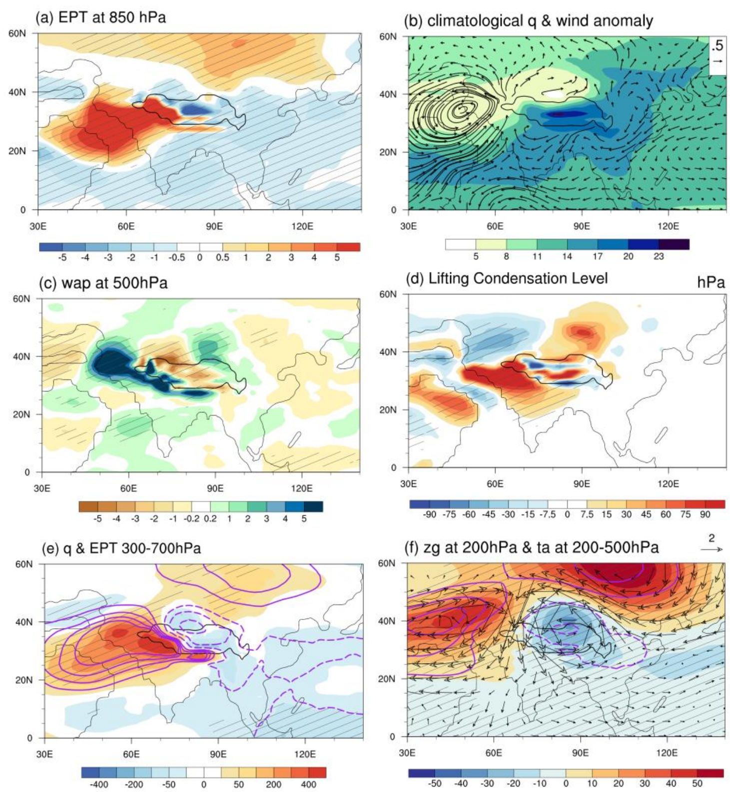

Figure 7. The differences of JJA mean thermal dynamical and dynamical variables between IP0HM0 and IP100HM100 simulations. (a) Equivalent Potential temperature (EPT, shading, unit: K) at 850 hPa; (b) climatological specific humidity (shading, g kg^{-1}) and wind differences (vector, unit: m s^{-1}) at 850 hPa; (c) vertical velocity in pressure coordinate (-10^{-2} Pa s^{-1}) at 500 hPa; (d) Lifting condensation level (LCL, unit: hPa, positive value represent lower LCL); (e) Specific humidity (shading) and EPT (contours, unit: K) integrated between 300 and 700 hPa; (f) geopotential height (shading, unit: m) and wind (vector, unit: m s^{-1}) at 200 hPa.

https://doi.org/10.5194/cp-2022-76
Preprint. Discussion started: 18 November 2022

Climate of the Past Discussions

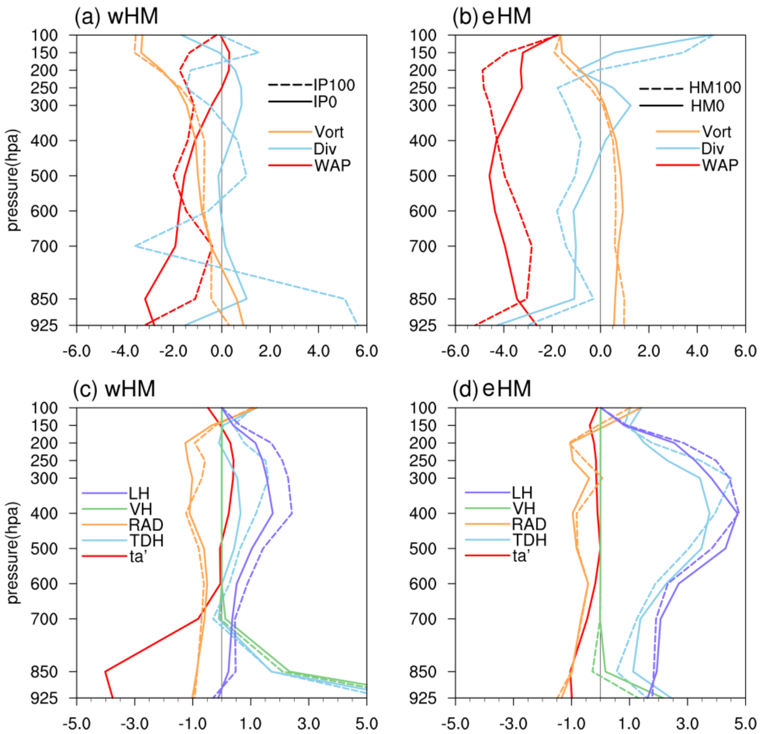

Figure 8. Vertical profile of (a-b) dynamical variables and (c-d) thermodynamical variables at (a, c) west of HM (wHM, 65°E, 28°N) and (b, d) east of HM (eHM; 80°E, 25°N). The dynamical variables are JJA mean vorticity (Vort; orange lines, 10^{-5} s^{-1}), divergence (Div; blue lines,10^{-6} s^{-1}) and vertical velocity (WAP; red lines, 10^{-2} Pa s^{-1}) in IP/HM0 (solid lines) and IP/HM100 (dashed lines). The thermodynamical variables are JJA mean latent heating (LH, purple lines), vertical diffusion heating (VH, green lines), radiative heating (RAD, orange lines) and total diabatic heating (TDH, blue lines) in IP/HM0 (solid lines) and IP/HM100 (dashed lines). Unit is k day^{-1}. The changes in temperature between IP100 and IP0 are plotted as solid red lines (unit: K).